



Title	Non-contact and non-destructive Lamb wave generation using laser-induced plasma shock wave
Author(s)	Hosoya, Naoki; Yoshinaga, Atsushi; Kanda, Atsushi; Kajiwara, Itsuro
Citation	International journal of mechanical sciences, 140, 486-492 <a href="https://doi.org/10.1016/j.ijmecsci.2018.03.023">https://doi.org/10.1016/j.ijmecsci.2018.03.023</a>
Issue Date	2018-05
Doc URL	<a href="http://hdl.handle.net/2115/70914">http://hdl.handle.net/2115/70914</a>
Rights(URL)	<a href="https://creativecommons.org/licenses/by-nc-nd/4.0/">https://creativecommons.org/licenses/by-nc-nd/4.0/</a>
Type	article
File Information	1-s2.0-S0020740317326553-main.pdf



[Instructions for use](#)



Contents lists available at ScienceDirect

## International Journal of Mechanical Sciences

journal homepage: [www.elsevier.com/locate/ijmecsci](http://www.elsevier.com/locate/ijmecsci)

# Non-contact and non-destructive Lamb wave generation using laser-induced plasma shock wave

Naoki Hosoya<sup>a,\*</sup>, Atsushi Yoshinaga<sup>b</sup>, Atsushi Kanda<sup>c</sup>, Itsuro Kajiwara<sup>d</sup>

<sup>a</sup> Department of Engineering Science and Mechanics, Shibaura Institute of Technology, 3-7-5 Toyosu, Koto-ku, Tokyo 135-8548, Japan

<sup>b</sup> Division of Mechanical Engineering, Shibaura Institute of Technology, 3-7-5 Toyosu, Koto-ku, Tokyo 135-8548, Japan

<sup>c</sup> Aeronautical Technology Directorate, Japan Aerospace Exploration Agency, 6-13-1 Osawa, Mitaka-shi, Tokyo 181-0015, Japan

<sup>d</sup> Division of Human Mechanical Systems and Design, Hokkaido University, N13, W8, Kita-ku, Sapporo 060-8628, Japan

## ARTICLE INFO

## Keywords:

Lamb wave  
Non-destructive evaluation  
Laser-induced plasma  
Shock wave  
Acoustic wave  
Non-contact excitation

## ABSTRACT

This paper proposes a non-contact and non-destructive method to generate Lamb waves against a target structure using the impulse excitation force generated by laser-induced plasma (LIP). When a high power pulse laser is irradiated in air and its laser fluence exceeds  $10^{15}$  W/m<sup>2</sup>, a plasma is formed. While the plasma in air expands in high speed, shock waves on the spherical surface are generated and these shock waves become the impulse excitation force against a target structure, resulting in the non-contact and non-destructive approach. A 2024 aluminum alloy plate is used as the test piece in the experiment, and the dynamic characteristics of the Lamb waves generated from LIP shock waves are measured. Phase velocity and group velocity of generated Lamb waves were compared to the calculated values from Rayleigh-Lamb frequency equations and we found that maximum error was 5% and its frequency component included at least 400 kHz. Further, we investigated the relationship between the distance from the LIP shock wave-generating location to a test piece and the dynamic characteristics of the generated Lamb waves. This method can control the amplitude and the frequency components of generated Lamb waves by changing this distance.

© 2018 The Authors. Published by Elsevier Ltd.

This is an open access article under the CC BY-NC-ND license.

(<http://creativecommons.org/licenses/by-nc-nd/4.0/>)

## 1. Introduction

Lamb waves, which were discovered by Lamb in 1916, are guided waves that propagate in thin plates. Their characteristics include a small attenuation and propagation over long distances [1–5]. Further, fundamental features of Lamb waves and ultrasonic nondestructive evaluation are summarized by Su [6] and Kundu [7], respectively. Numerous studies on Lamb wave applications to detect damage in large structures such as airplanes, factories, and ships are underway. Lamb wave generation techniques can be divided into two main categories: those using a contact-type device (e.g., piezoelectric zirconate titanate) [8–21] and those using a non-contact type device [22–38]. Damage detection using a contact-type device seems inefficient, but inserting the device into a target structure can improve the efficiency. However, it is difficult to generate Lamb waves by a contact-type device when the target structure is in a high temperature environment or submerged in liquid. Hence, the generation of Lamb waves using a non-contact type device is being considered.

Non-contact type devices include air-coupled transducers [37,38] and laser thermoelasticities [22–36]. The former involves placing an air-coupled transducer near the Lamb wave generation point on the target structure, and the vibration of the transducer is transmitted through the medium (air in this case). The latter type of device irradiates a pulse laser beam at the generation point of Lamb waves on the target structure, causing instantaneous heat expansion and constriction in the applied area due to changes in the temperature that produce non-contact excitation. Lamb waves generated by a laser thermoelasticity device have much smaller amplitudes than those generated by a contact-type device (about a few hundred picometers), resulting in measurements with a lower signal-to-noise (SN) ratio. The threshold of laser thermoelasticity also changes, depending on the laser beam-irradiated material, laser fluence, wavelength of the laser beam, or polarization, making it extremely difficult to determine the threshold value.

When the laser fluence reaches  $10^{12}$ – $10^{14}$  W/m<sup>2</sup>, laser ablation (LA) forms [39–49]. LA is the formation of a high-temperature high-

\* Corresponding author.

E-mail addresses: [hosoya@sic.shibaura-it.ac.jp](mailto:hosoya@sic.shibaura-it.ac.jp) (N. Hosoya), [md15093@shibaura-it.ac.jp](mailto:md15093@shibaura-it.ac.jp) (A. Yoshinaga), [kanda@chofu.jaxa.jp](mailto:kanda@chofu.jaxa.jp) (A. Kanda), [ikajiwara@eng.hokudai.ac.jp](mailto:ikajiwara@eng.hokudai.ac.jp) (I. Kajiwara).

<https://doi.org/10.1016/j.ijmecsci.2018.03.023>

Received 20 September 2017; Received in revised form 9 March 2018; Accepted 17 March 2018

Available online 19 March 2018

0020-7403/© 2018 The Authors. Published by Elsevier Ltd. This is an open access article under the CC BY-NC-ND license. (<http://creativecommons.org/licenses/by-nc-nd/4.0/>)

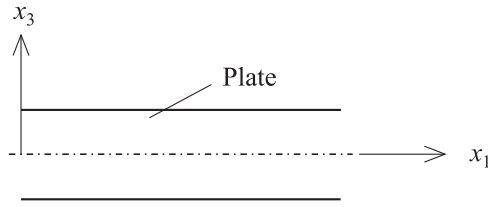


Fig. 1. Geometry of the free plate problem.

density plasma plume from a laser-irradiated surface. When a plasma plume of mass  $\Delta m$  is released by velocity  $v$ , the gained momentum (impulse) is  $\Delta mv$  and this becomes the excitation force against a target structure. LA has been researched for vibration tests [40–47,49], laser vapor deposition [50], thrust [51], laser micromachining [52], laser peening [53], detection of bolt loosening [42], and acoustic tests [48]. It is a newly established as non-contact excitation technology [40–49], but it is destructive as sub-millimeter damage is generated on the target structure. Regardless, studying the amplitude levels and modes of Lamb waves using LA is extremely valuable.

For this reason, we have shown that Lamb waves generated by LA against a 2024 aluminum alloy plate contain frequency components up to about 400 kHz and an amplitude of about 20 nm. By observing the propagation of these Lamb waves, we have also demonstrated that damage detection is possible [46]. If we could generate non-contact and non-destructive Lamb waves against a target structure, which have about the same level of amplitude as that of the conventional methods, the field of damage detection using Lamb waves may advance even further.

This paper proposes a non-contact and non-destructive method to generate Lamb waves against a target structure using the impulse excitation force generated by laser-induced plasma (LIP) [54–63]. Generation of non-contact and non-destructive Lamb waves should contribute tremendously to the development of damage detection technologies for large structures. When a high power pulse laser is irradiated in air and its laser fluence exceeds  $10^{15}$  W/m<sup>2</sup>, a plasma is formed. When this plasma expands into a spherical shape, shock waves are generated. We use these shock waves as the non-contact and non-destructive excitation force against a target structure. We show that the shock waves can be used to measure the frequency response functions [61], to detect damages or to suppress vibrations in a membrane structure [58,62] and to evaluate the firmness of apples [63].

In this experiment, we use a 2024 aluminum alloy plate as the test piece, and measure the dynamic characteristics of the Lamb waves generated from LIP shock waves (amplitude, frequency response, phase velocity, and group velocity). We also investigate the relationship between the distance from the LIP shock wave-generating location to a test piece (hereafter called the standoff distance or  $d$ ) and the dynamic characteristics of the generated Lamb waves. This study demonstrates that, within a standoff distance range of 5–40 mm, Lamb waves suitable for damage detection can be produced. Previous research [54–63] has not employed LIP shock waves as the impulse excitation force to generate Lamb waves. Furthermore, the dynamic characteristics of the lamb waves generated by LIP shock waves have yet to be controlled by changing the standoff distances in the previous research [54–63], even though it is expected that an amplitude, a frequency band and an excitation area of the impulse excitation force generated by LIP shock waves can be adjusted by changing the standoff distance.

## 2. Lamb wave

The equations for a longitudinal wave and a transverse wave on a flat plate under the strained condition shown in Fig. 1 are

$$\frac{\partial^2 \varphi}{\partial x_1^2} + \frac{\partial^2 \varphi}{\partial x_3^2} = \frac{1}{c_L^2} \frac{\partial^2 \varphi}{\partial t^2} \quad (1)$$

$$\frac{\partial^2 \psi}{\partial x_1^2} + \frac{\partial^2 \psi}{\partial x_3^2} = \frac{1}{c_T^2} \frac{\partial^2 \psi}{\partial t^2}$$

where  $\varphi$  and  $\psi$  are the potential,  $c_L$  is the velocity of the longitudinal wave, and  $c_T$  is the velocity of the transverse wave. By solving Eq. (1), we can obtain the Rayleigh–Lamb frequency equations.

For symmetric modes

$$\frac{\tan(qh)}{\tan(ph)} = -\frac{4k^2 pq}{(q^2 - k^2)^2} \quad (2)$$

For antisymmetric modes

$$\frac{\tan(qh)}{\tan(ph)} = -\frac{(q^2 - k^2)^2}{4k^2 pq} \quad (3)$$

and

$$p^2 = \frac{\omega^2}{c_L^2} - k^2 \quad (4)$$

$$q^2 = \frac{\omega^2}{c_T^2} - k^2 \quad (5)$$

$$k = \frac{\omega}{c_p} \quad (6)$$

where  $k$  is the wave number,  $\omega$  is the angular frequency of the Lamb wave, and  $c_p$  is the phase velocity of the Lamb wave mode. In this paper, we calculate the phase and group velocities of the Lamb waves from these equations.

## 3. Lamb wave generation using LIP shock wave

### 3.1. Lamb wave generation system

Fig. 2 shows the Lamb wave generation system using a LIP shock wave [49,54–63]. A laser beam from a Nd:YAG pulse laser (Continuum, Continuum surelite III-10: wavelength, 1064 nm; beam diameter, 9.5 mm; pulse width, 5 ns; maximum output power, 1 J; beam divergence angle, 0.5 mrad) installed on the optical surface plate becomes condensed by a plano-convex lens and exceeds the threshold of the laser fluence by LIP formation in air. Ideally, LIP shock waves are generated at the focus of the plano-convex lens. In this experiment, the laser pulse energy is 1 J and the focal distance of a plano-convex lens is 200 mm (Fig. 2(b) and (c)), generating LIP shock waves directly on top of the excitation point of the test piece. Four different values of  $d$  are observed: 5 mm, 10 mm, 20 mm, and 40 mm (Fig. 2(d)). The test piece is a 2024 aluminum alloy plate measuring 400 mm × 400 mm × 2 mm. There are two Lamb wave measurement areas: case A, in which the right end of the measurement area is 50 mm away from the excitation point, and case B, in which the measurement area is directly under the excitation point. In this experiment, a single axis scanning laser Doppler vibrometer (SLDV) (Polytec, PSV-500: He-Ne laser; measurement velocity, 0–20 m/s; sampling max, 5.12 MHz) is used to measure the vibration components in the out-of-plane direction of the test piece inside a 100 mm × 100 mm area in 2 mm intervals. The number of sampling points, the sampling frequency, and the average number of measurements are 2048, 2.56 MHz, and 10, respectively. To prevent spike noise in the measurement, 0–400 kHz band pass filter is applied. Thus, the  $A_0$  mode is the target measurement of the Lamb mode in this experiment.

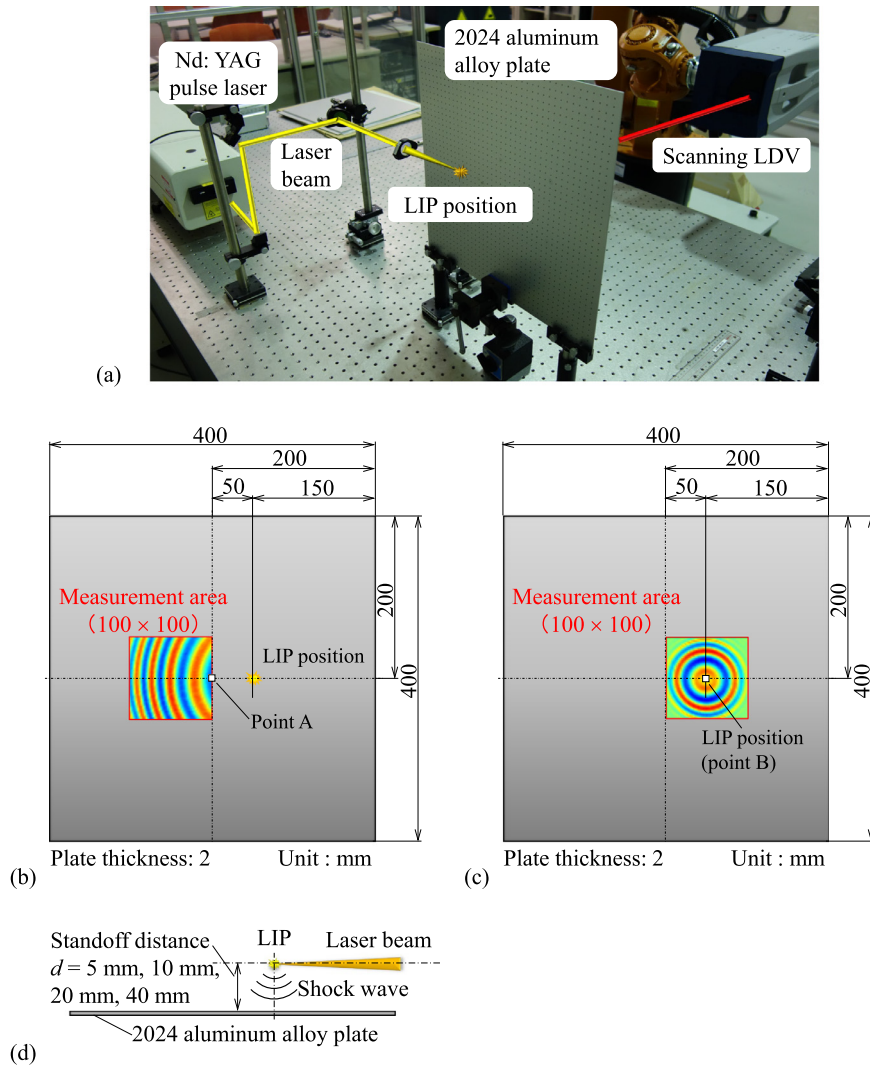


Fig. 2. Non-contact and non-destructive laser excitation systems for Lamb wave generation using LIP. (a) Experimental systems for Lamb wave generation, (b) case A, (c) case B and (d) standoff distance.

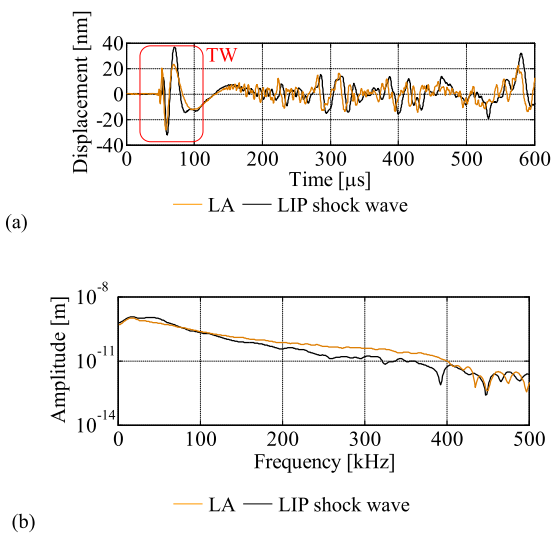


Fig. 3. Measured Lamb waves generated by LA (orange line) and LIP shock wave (black line). (a) Time responses and (b) power spectra.

### 3.2. Measured Lamb wave

Fig. 3 shows the time-history waveform of the Lamb wave using LIP with a standoff distance of 5 mm at point A (refer to Fig. 2(b)) and its Fourier spectra. Fig. 4 shows the propagation of the Lamb wave. Fig. 3(b) is the result of the Fourier transformation of part of the time waveform in Fig. 3(a) where the reflection of the wave from the boundary does not overlap. (This is denoted by “TW” in Fig. 3(a).) In Figs. 3 and 4, the Lamb wave generated by LA (laser pulse energy 500 mJ) is also shown for comparison. Fig. 3(a) shows that the shapes of the LIP and LA Lamb waves match qualitatively. However, the LIP Lamb wave has a much higher amplitude but a slower arrival time than the LA Lamb wave. The cause of the former is attributed to a larger laser pulse energy of LIP compared to LA (LIP, 1 J; LA, 500 mJ). The latter is due to the time required before the excitation force takes effect on the test piece after the LIP shock waves propagate to the excitation point (LA applies the excitation force directly to the test piece). Fig. 3(b) shows that both LA and LIP include frequency components of up to about 400 kHz, which is the band pass filter’s upper limit frequency, but LIP has fewer frequency components exceeding 100 kHz than LA. By adjusting the standoff distance, the excitation force on the test piece generated by LIP Lamb waves can be changed in terms of the frequency component, strength, and area, as illustrated in the next chapter.

**Table 1**  
Phase velocity of LIP shock wave generated Lamb wave.

Center frequency (Frequency band) [kHz]	Phase velocity [km/s]				
	Measured (LIP)	Measured (LA)	Calculated	Error (LIP) [%]	Error (LA) [%]
25 (0–50)	–	–	0.69	–	–
75 (50–100)	1.10	1.15	1.15	–5%	0%
125 (100–150)	1.40	1.45	1.44	–3%	1%
175 (150–200)	1.69	1.69	1.65	2%	2%
225 (200–250)	1.87	1.86	1.82	3%	2%
275 (250–300)	1.98	1.98	1.95	2%	2%
325 (300–350)	2.11	2.09	2.07	2%	1%
375 (350–400)	2.20	2.18	2.16	2%	1%

**Table 2**  
Group velocities of LIP shock wave generated Lamb wave.

Center frequency (Frequency band) [kHz]	Group velocity [km/s]				
	Measured (LIP)	Measured (LA)	Calculated	Error (LIP) [%]	Error (LA) [%]
25 (0–50)	–	–	1.21	–	–
75 (50–100)	2.13	2.12	2.03	5%	4%
125 (100–150)	2.52	2.53	2.44	3%	4%
175 (150–200)	2.73	2.70	2.67	2%	1%
225 (200–250)	2.95	2.90	2.82	4%	3%
275 (250–300)	3.03	3.00	2.90	4%	3%
325 (300–350)	3.11	3.08	3.01	3%	2%
375 (350–400)	3.12	3.10	3.05	2%	2%

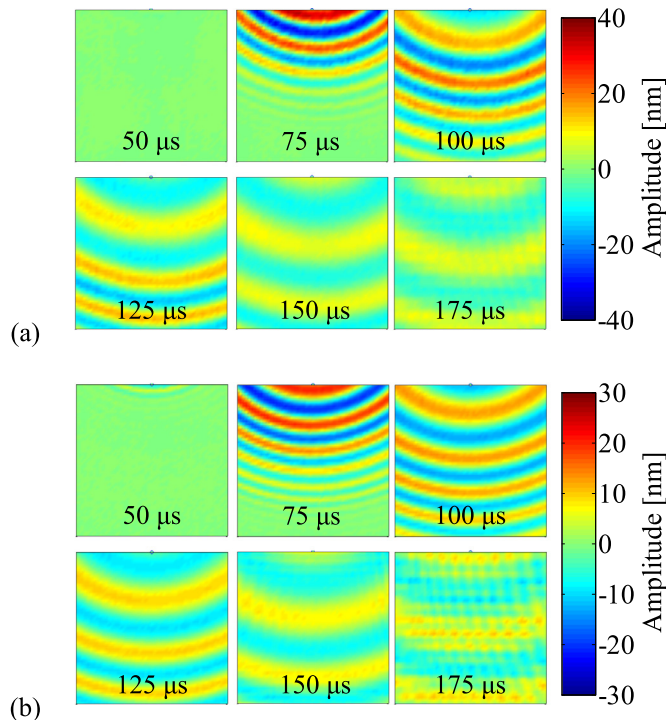


**Fig. 4.** Lamb wave propagation in the entire measurement area (100 mm × 100 mm): 50 μs, 75 μs, 100 μs, 125 μs, 150 μs and 175 μs. (a) The LIP Lamb wave and (b) the LA Lamb wave.

We compared and evaluated the  $A_0$  mode phase and the group velocities obtained from this method to the results of the Rayleigh–Lamb frequency equations. This paper obtains the  $A_0$  mode phase and group velocities using the following steps [46].

- (i) By applying a digital filter to the frequency spectra obtained by Fourier transform of Lamb waves' time history waveforms for all measurement points, the frequency components are extracted every 50 kHz and an inverse Fourier transformation is used to obtain the time-history waveforms filtered by a digital filter.
- (ii) Based on the time-history waveforms at all measurement points generated in (i), wave propagation figures (Fig. 4) can be produced. Wave propagation figures are placed at each time stamp in the depth direction (perpendicular to the direction of every measurement point). By cutting at an arbitrary cross section (this paper used the middle of the measurement area containing point A), the cross-section image is obtained with time in the x-axis and the distance in the y-axis. Lamb waves appear as a trajectory in the cross-section image. Hence, the phase and the group velocities of the Lamb waves can be obtained from the slope.
- (iii) The phase and group velocities are obtained in every frequency bandwidth by repeating steps (i) and (ii) every 50 kHz up to the limit frequency of the band pass filter at 400 kHz.

Fig. 5 shows the  $A_0$  mode dispersion curves of the phase and group velocities as well as those at every frequency band obtained by this method plotted on the analytically generated dispersion curve. Tables 1 and 2 show the phase velocity and the group velocity, respectively, at every frequency band obtained by the analytical method and this method. For comparison, these figures and tables include the phase and group velocities obtained by LA. From these results, we can conclude that the error of the phase and group velocities of the Lamb wave obtained by this method is within 5% and the precision is about the same as the LA Lamb wave. This paper also measures the phase and group velocities every 50 kHz, which causes additional error in the data.

### 3.3. Effect of standoff distance on LIP shock wave generated Lamb wave

We investigated the effect of the standoff distance on the amplitude and frequency components of the Lamb waves generated by LIP shock waves. The larger the standoff distance, the easier the measurement setup becomes, improving the usability of this method. As for the

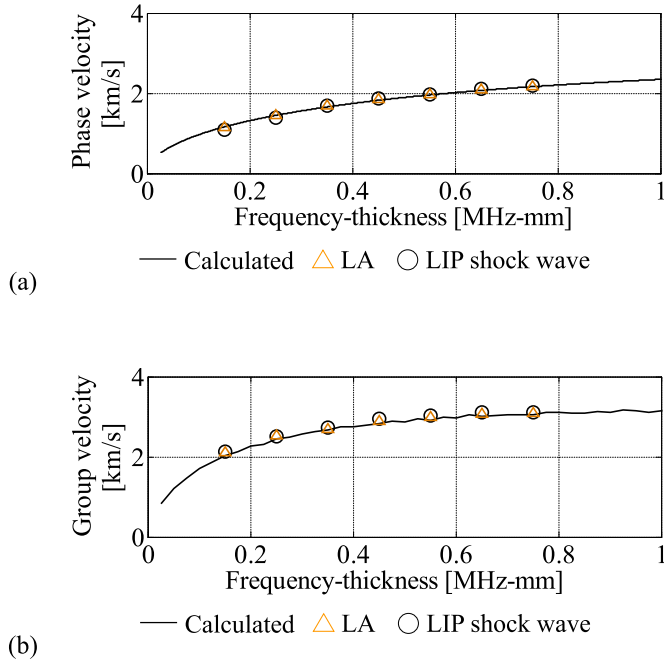


Fig. 5. Comparison between the Lamb wave propagation velocity of the  $A_0$  mode generated by LA and the calculated propagation velocity: calculated by theory, generated by LA (orange triangle) and LIP shock wave (black circle). (a) Phase velocity and (b) group velocity.

LIP shock wave (Eq. (7)), the pressure of LIP shock waves (strength of the excitation force) is inversely proportional to the third power of the propagation distance. When the propagation velocity of the shock waves becomes equal to that of the acoustic wave (Eq. (10)) (when it propagates as an acoustic wave), the pressure of the acoustic wave is inversely proportional to the propagation distance. Hence, it is crucial to investigate the relationships among the standoff distance, the amplitude and frequency components of the generated Lamb waves to identify the applicable range of this method. Whether using a LIP shock wave or treating it as an acoustic wave, the pressure, propagation velocity, and arrival time can be expressed by the following equations [56]

Shock wave

$$P^{sh}(d) = \left(\frac{2}{5}\right)^2 \frac{2\zeta_0^5}{\gamma + 1} E d^{-3} \quad (7)$$

$$v^{sh}(d) = \frac{2}{5} \zeta_0^{5/2} \left(\frac{E}{\rho_0}\right)^{1/2} d^{-3/2} \quad (8)$$

$$r_0^{sh}(d) = \left(\frac{d}{\zeta_0}\right)^{5/2} \left(\frac{\rho_0}{E}\right)^{1/2} \quad (9)$$

Acoustic wave

$$P^{ac}(d) = \left(\frac{2}{5}\right)^2 \frac{2\zeta_0^5}{\gamma + 1} \frac{E}{r_0^2 d} \quad (10)$$

$$v^{ac}(d) = v_0 = 340 \text{ m/s} \quad (11)$$

$$r_0^{ac}(d) = r_0^{sh}(r_0) + (d - r_0)/v_0 \quad (12)$$

where  $E$  [J] is the instantaneously released energy.  $\rho_0$  [kg/m<sup>3</sup>] is the density of the air and  $\gamma$  (~1.41) is the ratio of specific heat capacity.  $\zeta_0$  (~0.93) is a dimensionless quantity.  $d$  [m] is the standoff distance, and  $r_0$  [m] is the distance when the velocity of the shock wave is equal to that of the acoustic wave. In this experiment,  $r_0 = 9.3$  mm.

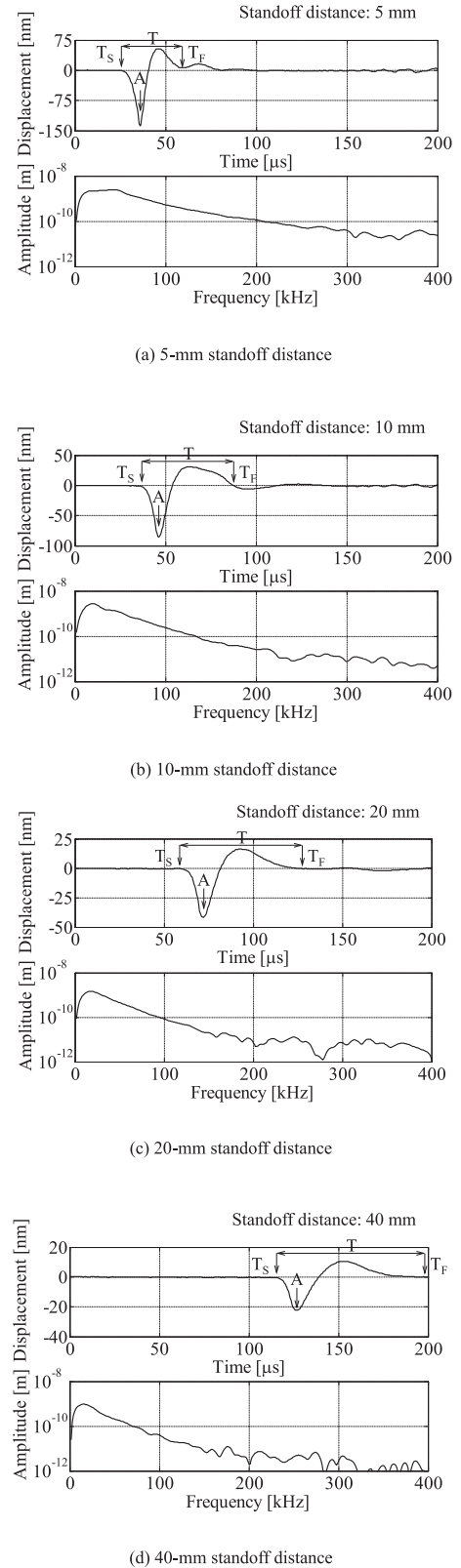


Fig. 6. Time responses and power spectra of measured directly under the LIP shock waves with standoff distances of 5 mm, 10 mm, 20 mm, and 40 mm. (a) 5-mm standoff distance, (b) 10-mm standoff distance, (c) 20-mm standoff distance and (d) 40-mm standoff distance.

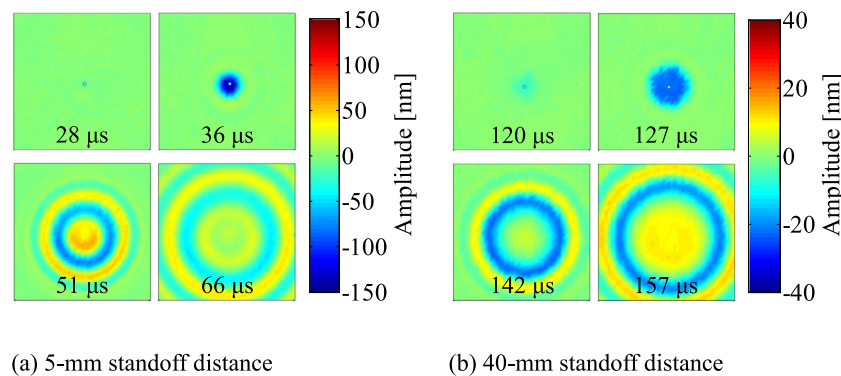


Fig. 7. Lamb wave propagation in the measurement area (100 mm × 100 mm) with standoff distances of 5 mm and 40 mm. (a) 5-mm standoff distance and (b) 40-mm standoff distance.

Fig. 6 shows the Lamb wave time-history response and the power spectrum measured directly under the LIP shock waves (Fig. 2(c)) with standoff distances of 5 mm, 10 mm, 20 mm, and 40 mm. As the standoff distance becomes larger, (i) the arrival time of a Lamb wave becomes longer, (ii) the amplitude of the measured Lamb wave becomes smaller, and (iii) the frequency components included in the Lamb wave become lower. Observation (i) is related to the time that a shock wave or acoustic wave propagates to the surface of the test piece. The cause of (ii) may be due to the smaller pressure of the LIP shock wave or the acoustic wave (excitation input strength) as it propagates (Eq. (7) or Eq. (10)). The amplitude of the generated Lamb wave is proportional to the excitation input force. The pressure of the LIP shock wave is inversely proportional to the third power of the propagation distance and the acoustic wave pressure is inversely proportional to the propagation distance. For example, if the standoff distance is 10 mm, 20 mm, or 40 mm, the absolute value of the Lamb wave amplitude ('A' in Fig. 6) is 85.6 nm, 41.6 nm, or 22.2 nm, respectively. These values are inversely proportional to the propagation distance (excluding the standoff distance at 5 mm within the shock wave area from this comparison). As for (iii), when the propagation distance of the LIP shock waves or the acoustic waves increases, both the pressure and pulse amplitude (length between 'T<sub>S</sub>' and 'T<sub>F</sub>' in Fig. 6 is defined as 'T') are affected, increasing the amplitude, but decreasing the high frequency components in the excitation force.

Fig. 7 shows wave propagation at four different times in Fig. 6 ('T<sub>S</sub>', 'A', 15 μs after 'A', and 30 μs after 'A'). Fig. 7(a) and (b) are for standoff distances of 5 mm and 40 mm, respectively. Considering the measured data contains noise floor with a mean of 0.2 nm, 'T<sub>S</sub>' was set to the time when the absolute value of the amplitude of the Lamb wave exceeds 5 nm, which is sufficient to avoid the noise effect. 'A' was set to the time when the absolute value of the amplitude of the Lamb wave was maximized. Wave propagation of both waves qualitatively matches and produces Lamb waves directly under LIP. As a result, we conclude that Lamb waves can be generated in the range of the standoff distance in this experiment (5–40 mm). Although LIP shock waves and acoustic waves propagate into a spherical shape and generate an excitation force against a target structure, further studies on the excitation area are necessary.

#### 4. Conclusions

This paper proposes a non-contact and non-destructive method to generate Lamb waves using LIP shock waves. In this method, irradiating a high power Nd:YAG pulse laser near the excitation point of the target structure forms a LIP, and the shock waves generated when the plasma expands at high speed act as the impulse excitation force against the target structure. In this experiment, we employ SLDV, which can only measure the out-of-plane direction, and a 0–400 kHz band pass filter to remove spike noise during the measurements. Hence, the measured Lamb waves are the A<sub>0</sub> mode. The Lamb waves generated by this method

include frequency components up to 400 kHz. By comparing the phase and the group velocities of the Lamb waves obtained by this method and the theoretical values from Rayleigh–Lamb frequency equations, the maximum error is 5%.

To improve usability of this method, we studied the impact of the standoff distance on the generated Lamb waves. As the standoff distance increases, more time is necessary to produce a Lamb wave due to the increase in the propagation distance of LIP shock wave, the amplitude of the Lamb wave decreases and the frequency components in the Lamb wave become lower. However, within a standoff distance range of 5–40 mm, which was employed in this experiment, Lamb waves suitable for damage detection can be produced. And this method can control the amplitude and the frequency components of generated Lamb waves by changing the standoff distance.

If this method is applied to detect damage for target structures, this method is more suitable for a large area damage inspection on colossal structures such as an aircraft. Therefore, a size of target detectable damage will become macroscopic damage. And a detectable size of damage using our method is limited from the viewpoint of the wave length of Lamb waves. However, to detect a smaller damage using our method, we may need to investigate a wave length, a pulse width, energy of laser beam for generating LIP shock wave. In addition, a spatial resolution in LDV measurements of a target structure to be inspected should be improved.

#### Acknowledgements

We thank the Japan Society for the Promotion of Science for their support under the Grants-in-Aid for Scientific Research programs (Grants-in-Aid for Scientific Research (B), Grant No. JP16H04291 and No. JP16H04286, and Grants-in-Aid for Challenging Exploratory Research, Grant No. JP26630080 and JP17K18858).

#### References

- [1] Lamb H. On waves in an elastic plate. *Philos R Soc A–Math Phys* 1917;93(648):114–128.
- [2] Rose JL. *Ultrasonic waves in solid media*. Cambridge: Cambridge University Press; 2004.
- [3] Su Z, Ye L, Lu Y. Guided Lamb waves for identification of damage in composite structures: a review. *J Sound Vib* 2006;295(3–5):753–780.
- [4] Giurgiutiu V, Soutis C. Enhanced composites integrity through structural health monitoring. *Appl Compos Mater* 2012;19(5):813–829.
- [5] Mitra M, Gopalakrishnan S. Guided wave based structural health monitoring: a review. *Smart Mater Struct* 2016;25(5):053001.
- [6] Su Z, Ye L. *Fundamentals and analysis of Lamb waves. identification of damage using Lamb waves*. Lecture notes in applied and computational mechanics 2009;48.
- [7] Kundu T. *Ultrasonic nondestructive evaluation: engineering and biological material characterization*. 1st edition. Florida: CRC press; 2003.
- [8] Bourasseau N, Moulin E, Delebarre C, Bonnau P. Radome health monitoring with Lamb waves: experimental approach. *NDT&E Int* 2000;33(6):393–400.

- [9] Cernadas D, Trillo C, Doval ÁF, López Ó, López C, Dorrió BV, Fernández JL, Pérez-Amor M. Non-destructive testing of plates based on the visualisation of Lamb waves by double-pulsed TV holography. *Mech Syst Signal Pr* 2006;20(6):1338–1349.
- [10] Staszewski WJ, Lee BC, Traynor R. Fatigue crack detection in metallic structures with Lamb waves and 3D laser vibrometry. *Meas Sci Technol* 2007;18(3):727–39.
- [11] Bermes C, Kim JY, Qu J, Jacobs LJ. Nonlinear Lamb waves for the detection of material nonlinearity. *Mech Syst Signal Pr* 2008;22(3):638–646.
- [12] Harri K, Guillaume P, Vanlanduit S. On-line damage detection on a wing panel using transmission of multisine ultrasonic waves. *NDT & E Int* 2008;41(4):312–317.
- [13] Staszewski WJ, Mahzan S, Traynor R. Health monitoring of aerospace composite structures – active and passive approach. *Compos Sci Technol* 2009;69(11–12):1678–85.
- [14] Giridhara G, Rathod VT, Naik S, Mahapatra DR, Gopalakrishnan S. Rapid localization of damage using a circular sensor array and Lamb wave based triangulation. *Mech Syst Signal Pr* 2010;24(8):2929–2946.
- [15] Lammering R. Observation of piezoelectrically induced Lamb wave propagation in thin plates by use of speckle interferometry. *Exp Mech* 2010;50(3):377–387.
- [16] Watkins R, Jha R. A modified time reversal method for Lamb wave based diagnostics of composite structures. *Mech Syst Signal Pr* 2012;31:345–54.
- [17] Rogge MD, Leckey CAC. Characterization of impact damage in composite laminates using guided wavefield imaging and local wavenumber domain analysis. *Ultrasonics* 2013;53:1217–26.
- [18] Liu Y, Goda R, Samata K, Kanda A, Hu N, Zhang J, Ning H, Wu L. An efficient algorithm embedded in an ultrasonic visualization technique for damage inspection using the AE sensor excitation method. *Sensors* 2014;14(11):20439–50.
- [19] Senyurek VY. Detection of cuts and impact damage at the aircraft wing slot by using Lamb wave method. *Measurement* 2015;67:10–23.
- [20] Yu L, Tian Z, Leckey CAC. Crack imaging and quantification in aluminum plates with guided wave wavenumber analysis methods. *Ultrasonics* 2015;62:203–212.
- [21] Mesnil O, Ruzzene M. Sparse wavefield reconstruction and source detection using compressed sensing. *Ultrasonics* 2016;67:94–104.
- [22] Dewhurst RJ, Edwards C, McKie ADW, Palmer SB. Estimation of the thickness of thin metal sheet using laser generated ultrasound. *Appl Phys Lett* 1987;51(14):1066–8.
- [23] Pierce SG, Culshaw B, Philp WR, Lecuyer F, Farlow R. Broadband Lamb wave measurements in aluminium and carbon/glass fibre reinforced composite materials using non-contacting laser generation and detection. *Ultrasonics* 1997;35(2):105–14.
- [24] Gao W, Glorieux C, Thoen J. Laser ultrasonic study of Lamb waves: determination of the thickness and velocities of a thin plate. *Int J Eng Sci* 2003;41(2):219–28.
- [25] Silva MZ, Gouyon R, Lepoutre F. Hidden corrosion detection in aircraft aluminum structures using laser ultrasonics and wavelet transform signal analysis. *Ultrasonics* 2003;41(4):301–5.
- [26] Lee JR, Takatsubo J, Toyama N, Kang DH. Health monitoring of complex curved structures using an ultrasonic wavefield propagation imaging system. *Meas Sci Technol* 2007;18(12):3816–24.
- [27] Yashiro S, Takatsubo J, Toyama N. An NDT technique for composite structures using visualized Lamb-wave propagation. *Compos Sci Technol* 2007;67(15–16):3202–8.
- [28] Lee JR, Yoon CY. Development of an optical system for simultaneous ultrasonic wave propagation imaging at multi-points. *Exp Mech* 2010;50(7):1041–9.
- [29] Dixon S, Burrows SE, Dutton B, Fan Y. Detection of cracks in metal sheets using pulsed laser generated ultrasound and EMAT detection. *Ultrasonics* 2011;51(1):7–16.
- [30] Lee JR, Chia CC, Shin HY, Park CY, Yoon DJ. Laser ultrasonic propagation imaging method in the frequency domain based on wavelet transformation. *Opt Laser Eng* 2011;49(1):167–75.
- [31] Lee JR, Shin HJ, Chia CC, Dhital D, Yoon DJ, Huh YH. Long distance laser ultrasonic propagation imaging system for damage visualization. *Opt Laser Eng* 2011;49(12):1361–71.
- [32] Cès M, Royer D, Prada C. Characterization of mechanical properties of a hollow cylinder with zero group velocity Lamb modes. *J Acoust Soc Am* 2012;132(1):180–5.
- [33] Balvantín A, Baltazar A, Aranda-Sanchez JI. A study of guided wave propagation on a plate between two solid bodies with imperfect boundary conditions. *Int J Mech Sci* 2012;63(1):66–73.
- [34] Nishino H, Tanaka T, Yoshida K, Takatsubo J. Simultaneous measurement of the phase and group velocities of Lamb waves in a laser-generation based imaging method. *Ultrasonics* 2012;52(4):530–5.
- [35] Flynn EB, Chong SY, Jarmer GJ, Lee JR. Structural imaging through local wavenumber estimation of guided waves. *NDT&E Int* 2013;59:1–10.
- [36] Liu W, Hong JW. Modeling of three-dimensional Lamb wave propagation excited by laser pulses. *Ultrasonics* 2015;55:113–22.
- [37] Castaings M, Hosten B. Ultrasonic guided waves for health monitoring of high-pressure composite tanks. *NDT & E Int* 2008;41(8):648–55.
- [38] Harb MS, Yuan FG. A rapid, fully non-contact, hybrid system for generating Lamb wave dispersion curves. *Ultrasonics* 2015;61:62–70.
- [39] Torrisi L, Borrielli A, Margarone D. Study on the ablation threshold induced by pulse lasers at different wavelengths. *Nucl Instrum Meth B* 2007;255(2):373–9.
- [40] Kajiwara I, Hosoya N. Vibration testing based on impulse response excited by laser ablation. *J Sound Vib* 2011;330(21):5045–57.
- [41] Hosoya N, Kajiwara I, Hosokawa T. Vibration testing based on impulse response excited by pulsed-laser ablation: Measurement of frequency response function with detection-free input. *J Sound Vib* 2012;331(6):1355–65.
- [42] Huda F, Kajiwara I, Hosoya N, Kawamura S. Bolt loosening analysis and diagnosis by non-contact laser excitation vibration tests. *Mech Syst Signal Pr* 2013;40(2):589–604.
- [43] Hosoya N, Kajiwara I, Umenai K. Dynamic characterizations of underwater structures using non-contact vibration test based on nanosecond laser ablation in water: investigation of cavitation bubbles by visualizing shockwaves using the Schlieren method. *J Vib Control* 2016;22(17):3649–58.
- [44] Hosoya N, Umino R, Kajiwara I, Maeda S, Onuma T, Mihara A. Damage detection in transparent materials using non-contact laser excitation by nano-second laser ablation and high-speed polarization-imaging camera. *Exp Mech* 2016;56(2):339–43.
- [45] Hosoya N, Terashima Y, Umenai K, Maeda S. High spatial and temporal resolution measurement of mechanical properties in hydrogels by non-contact laser excitation. *AIP Adv* 2016;6 095223-1–095223-8.
- [46] Hosoya N, Umino R, Kanda A, Kajiwara I, Yoshinaga A. Lamb wave generation using nanosecond laser ablation to detect damage. *J Vib Control* 2017 Epub ahead of print 19 January 2017. doi:10.1177/1077546316687904.
- [47] Hosoya N, Kajiwara I, Umenai K, Maeda S. Dynamic characterizations of underwater structures using noncontact vibration tests based on nanosecond laser ablation in water: evaluation of passive vibration suppression with damping materials. *J Vib Control* 2017 Epub ahead of print 18 May 2017. doi:10.1177/1077546317710158.
- [48] Hosoya N, Kajiwara I, Inoue T, Umenai K. Non-contact acoustic tests based on nanosecond laser ablation: Generation of a pulse sound source with a small amplitude. *J Sound Vib* 2014;333(18):4254–64.
- [49] Kajiwara I, Hosoya N, inventor; National University Corporation Hokkaido University, Shibaura Institute of Technology, assignee. Method for measurement of vibration property of structure, and vibration property measurement device. United States Patent US 9,291,604 B2. 2011 Dec 22.
- [50] Qian F, Singh RK, Dutta SK, Pronko PP. Laser deposition of diamondlike carbon films at high intensities. *Appl Phys Lett* 1995;67:3120.
- [51] Yabe T, Phipps C, Yamaguchi M, Nakagawa R, Aoki K, Mine H, Ogata Y, Baasandash C, Nakagawa M, Fujiwara E, Yoshida K, Nishiguchi A, Kajiwara I. Microairplane propelled by laser driven exotic target. *Appl Phys Lett* 2002;80(23):4318–20.
- [52] Kamata M, Obara M, Gattass RR, Cerami LR, Mazur E. Optical vibration sensor fabricated by femtosecond laser micromachining. *Appl Phys Lett* 2005;87:051106.
- [53] Hatamleh O. Effects of peening on mechanical properties in friction stir welded 2195 aluminum alloy joints. *Mat Sci Eng A-struct* 2008;492(1–2):168–76.
- [54] Oksanen M, Hietanen J. Photoacoustic breakdown sound source in air. *Ultrasonics* 1994;32(5):327–331.
- [55] Wu B. High-intensity nanosecond-pulsed laser-induced plasma in air, water, and vacuum: a comparative study of the early-stage evolution using a physics-based predictive model. *Appl Phys Lett* 2008;93 doi:10.1104-1–101104-3.
- [56] Georgiev VB, Krylov VV, Qin Q, Attenborough K. Generation of flexural waves in plates by laser-initiated airborne shock waves. *J Sound Vib* 2011;330(2):217–28.
- [57] Hosoya N, Nagata M, Kajiwara I. Acoustic testing in a very small space based on a point sound source generated by laser-induced breakdown: stabilization of plasma formation. *J Sound Vib* 2013;332(19):4572–83.
- [58] Huda F, Kajiwara I, Hosoya N. Damage detection in membrane structures using non-contact laser excitation and wavelet transformation. *J Sound Vib* 2014;333(16):3609–24.
- [59] Bahr CJ, Zawodny NS, Bertolucci B, Li J, Sheplak M, Cattafesta LN. A plasma-based non-intrusive point source for acoustic beamforming applications. *J Sound Vib* 2015;344:59–80.
- [60] Eskelinen J, Hægström E, Delikaris-Manias S, Bolaños JG, Pulkki V. Beamforming with a volumetric array of massless laser spark sources – application in reflection tracking. *J Acoust Soc Am* 2015;137 EL389–EL395.
- [61] Hosoya N, Nagata M, Kajiwara I, Umino R. Nano-second laser-induced plasma shock wave in air for non-contact vibration tests. *Exp Mech* 2016;56(7):1305–11.
- [62] Zhang Y, Hiruta T, Kajiwara I, Hosoya N. Active vibration suppression of membrane structures and evaluation with a non-contact laser excitation vibration test. *J Vib Control* 2017;23(10):1681–92.
- [63] Hosoya N, Mishima M, Kajiwara I, Maeda S. Non-destructive firmness assessment of apples using a non-contact laser excitation system based on a laser-induced plasma shock wave. *Postharvest Biol Technol* 2017;128:11–17.